Received: 15 May 2024 | Accepted: 13 August 2024

DOI: 10.1002/pamm.202400094

RESEARCH ARTICLE

Acceleration of immersed computations of brittle phase-field fracture utilizing moment fitting schemes

Mahan Gorji | **Seyed Farhad Hosseini** | **Roman Sartorti** | **Lars Radtke** | **Alexander Düster**

Numerical Structural Analysis with Application in Ship Technology (M-10), Hamburg University of Technology, Hamburg, Germany

Correspondence
Mahan Gorji, Numerical Structural Analysis with Application in Ship Technology (M-10), Hamburg University of Technology, Am Schwarzenberg-Campus 4 (C), 21073 Hamburg, Germany.
Email: mahan.gorji@tuhh.de

Funding information
Deutsche Forschungsgemeinschaft, Grant/Award Numbers: DU 405/17, DU 405/21

Abstract

Numerical methods play an important role when predicting structural failure in industrial applications. Among various methods, the phase-field modeling (PFM) seems to be a very promising approach. By introducing an additional phase-field variable, it can account for crack initiation, crack propagation, dynamic crack branching and more. However, it needs a very fine mesh especially along the propagating crack path. When utilizing boundary-fitted methods such as the finite element method, this can lead to a large amount of elements and thus, results in huge systems of equations. In order to overcome this issue, immersed methods like the finite cell method (FCM) have been developed, where the mesh is independent of the geometry, which results in a fast and simple preprocessing. In this work, the FCM is applied to the PFM in order to simulate quasi-static brittle fracture of structures with complex geometries. Furthermore, the non-negative moment fitting (NNMF) is employed in order to accelerate the finite cell computations. The proposed methods are tested on a numerical example in order to demonstrate the strength of the NNMF.

1 | INTRODUCTION

The phase-field modeling (PFM) is very efficient when simulating failure such as fracture. It has been applied in different fields such as brittle fracture [1], ductile fracture [2], mixed-mode fracture [3], and dynamic fracture [4]. In contrast to the extended finite element method – another approach for simulating fracture – the crack is described smoothly, by introducing an additional scalar function called the phase-field. It interacts with the mechanical problem due to two mechanism, which are (I) the material degradation and (II) the strain energy driving force. In order to capture the solution in the vicinity of the crack path, a very fine mesh is required.

The finite element method (FEM) is very popular for structural mechanical problems. It utilizes a boundary-conforming mesh in order to discretize the structure. However, a very fine mesh is needed for fracture computations [1], which leads to huge computational costs and therefore, still remains a big challenge.

In recent years, immersed methods have gained more attention in the scientific community. They provide simple meshing strategies and thus, are qualified in order to circumvent the FEM drawbacks (Figure 1). Among different immersed methods, the finite cell method (FCM) is a well-known approach [5]. It utilizes a Cartesian grid in order to discretize

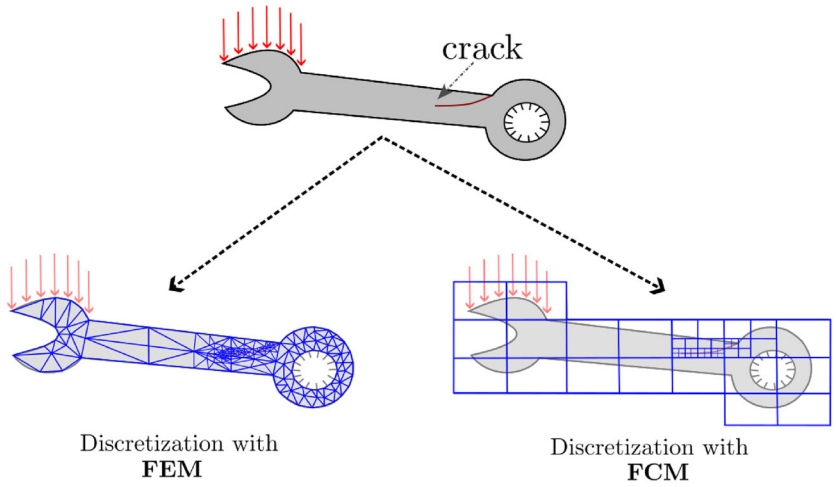

FIGURE 1 Different meshing approaches in structural mechanics: boundary-fitted methods (FEM) versus immersed method (FCM). FEM, finite element method.

the structure, employing high-order hierarchical shape functions on each of the so-called "finite cells." Furthermore, the multi-level *hp*-refinement can be applied in order to refine the FCM mesh towards the crack path [6, 7]. One advantage of the FCM is the possibility to utilize different geometry descriptions, such as level-set functions, boundary representation (B-rep, e.g., STL), voxel models, trimmed curves, or constructive solid geometries. Due to the non-conforming mesh however, discontinuities in the integrands of the stiffness matrices and load vectors occur, when the finite cells cut the domain boundary. This issue has been tackled by different integration schemes [8].

Usually, space-tree methods (such as quadtrees in 2D and octrees in 3D) are employed for the numerical integration, which are very robust and accurate [5]. However, they lead to a huge amount of integration points (IPs) and thus, are very expensive. On the other hand, moment fitting schemes are very promising, leading to a reduction of the integration effort [9]. In particular, the non-negative moment fitting (NNMF) has been proven to be very efficient for nonlinear FCM computations [10]. The idea is to derive an individual quadrature rule for each cut finite cell, where positivity of the weights is preserved.

In this work, the NNMF scheme is employed in FCM simulations of brittle phase-field fracture with the aim of reducing the computational effort, while the accuracy is maintained. Different numerical examples are investigated in order to show the efficiency of the proposed approaches.

The paper is structured as follows: Section 2 describes the theory of the PFM. Section 3 gives a brief introduction into the FCM as well as into the NNMF. In Section 4 numerical examples are studied. Finally, conclusions are provided in Section 5.

2 | PHASE-FIELD MODELING OF BRITTLE FRACTURE

2.1 | Basic formulation

The PFM is suited in order to simulate quasi-static brittle fracture. The main idea is to describe the crack by a smooth function, known as the *phase-field* $s(\boldsymbol{x})$. It acts as an indicator, that is, in the domain with no damage, $s = 0$, while in the region where the crack occurs, $s = 1$. In between, there is a transition zone, that is, $0 < s < 1$, which is controlled by the length-scale parameter ℓ. A structure is described by the domain Ω, on which body loads $\boldsymbol{b}$ are acting. Furthermore, displacements $\bar{\boldsymbol{u}}$ are prescribed on the Dirichlet boundary Γ_D and tractions $\bar{\boldsymbol{t}}$ are applied on the Neumann boundary Γ_N. The crack is represented by the boundary Γ_c (Figure 2A). According to ref. [11], the total potential energy is given as

$$\begin{aligned}\mathcal{E}_{\text{pot}}(\boldsymbol{u}) &= \int_{\Omega\setminus\Gamma_c} \Psi_e(\boldsymbol{u})\,\mathrm{d}\Omega + \int_{\Gamma_c} G_c\,\mathrm{d}\Gamma - \left(\int_{\Omega} \boldsymbol{b}\cdot\boldsymbol{u}\,\mathrm{d}\Omega + \int_{\Gamma_N} \bar{\boldsymbol{t}}\cdot\boldsymbol{u}\,\mathrm{d}\Gamma\right) \\ &= \mathcal{E}_{\text{el}}(\boldsymbol{u}) + \mathcal{E}_{\text{s}} - \mathcal{F}(\boldsymbol{u})\,.\end{aligned} \tag{1}$$

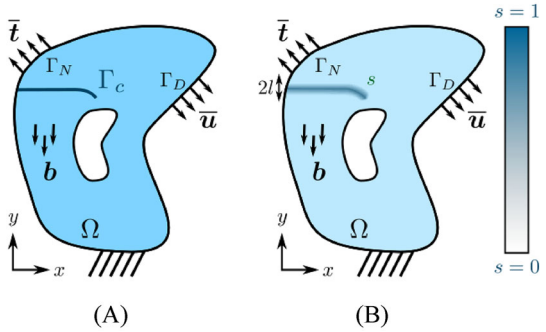

FIGURE 2 Concept of the PFM. Crack represented by (A) sharp boundary Γ_c, (B) smooth phase-field function s. PFM, phase-field modeling.

Here, the first term denotes the elastic energy $\mathcal{E}_{\text{el}}$, where Ψ_e is the strain energy density. Since a linear elastic material is assumed in this work, $\Psi_e = \frac{1}{2}\boldsymbol{\sigma}\cdot\boldsymbol{\varepsilon}$. Here, $\boldsymbol{\varepsilon}$ are the strains and $\boldsymbol{\sigma} = \mathbb{C}\,\boldsymbol{\varepsilon}$ the stresses, with the elasticity tensor $\mathbb{C}$. The unknown displacements are described by $\boldsymbol{u}$. The second term denotes the fracture surface energy $\mathcal{E}_{\text{s}}$, where G_c is the fracture toughness. Finally, the last term describes the work done by the external loads $\mathcal{F}$. So far the crack has been described by the sharp boundary Γ_c. When utilizing the PFM, the crack is represented smoothly by the phase-field s instead (Figure 2B). To this end, the regularization, as introduced by refs. [1, 12], is applied to the total energy, resulting in

$$\begin{aligned}\mathcal{E}_{\text{pot}}(\boldsymbol{u},s) &= \int_\Omega g(s)\,\Psi_e(\boldsymbol{u})\,\mathrm{d}\Omega + \int_\Omega G_c\left(\frac{w(s)}{2\ell} + \frac{\ell}{2}\,\nabla s\cdot\nabla s\right)\mathrm{d}\Omega - \left(\int_\Omega \boldsymbol{b}\cdot\boldsymbol{u}\,\mathrm{d}\Omega + \int_{\Gamma_N}\bar{\boldsymbol{t}}\cdot\boldsymbol{u}\,\mathrm{d}\Gamma\right)\\ &= \mathcal{E}_{\text{el}}(\boldsymbol{u},s) + \mathcal{E}_{\text{s}}(s) - \mathcal{F}(\boldsymbol{u})\,.\end{aligned} \tag{2}$$

Here, the elastic energy includes the degradation of the material, where $g(s) = (1-s)^2 + \kappa$ is the degradation function (with stability parameter $\kappa \ll 1$). Also the fracture surface energy is regularized, where $w(s) = s^2$ denotes the dissipation function. The variation of Equation (2) leads to

$$\delta\mathcal{E}_{\boldsymbol{u}}(\boldsymbol{u},s,\delta\boldsymbol{u}) = \int_\Omega g(s)\boldsymbol{\sigma}(\boldsymbol{u})\cdot\boldsymbol{\varepsilon}(\delta\boldsymbol{u})\,\mathrm{d}\Omega - \left(\int_\Omega \boldsymbol{b}\cdot\delta\boldsymbol{u}\,\mathrm{d}\Omega + \int_{\Gamma_N}\bar{\boldsymbol{t}}\cdot\delta\boldsymbol{u}\,\mathrm{d}\Gamma\right) = 0\,, \tag{3}$$

$$\delta\mathcal{E}_s(\boldsymbol{u},s,\delta s) = \int_\Omega g'(s)\Psi_e(\boldsymbol{u})\delta s\mathrm{d}\Omega + \int_\Omega G_c\left(\frac{w'(s)}{2\ell}\delta s + \ell\,\nabla s\,\nabla\delta s\right)\mathrm{d}\Omega = 0\,. \tag{4}$$

In order to consider that only tensile stresses contribute to the crack development, a strain energy split into tensile and compressive parts based on the volumetric-deviatoric decomposition is utilized [13]. Unfortunately, this violates the linear structure of the sub-problems later on. However, this issue is solved by utilizing the hybrid approach proposed by Ambati [14]. Furthermore, it has to be ensured, that damaged regions do not recover, that is irreversibility has to be enforced. To this end, a history-field is applied in this work [15, 16], which is given as

$$\mathcal{H}(\boldsymbol{x}) = \max_i\left\{\mathcal{H}_{i-1}(\boldsymbol{x}), \Psi_e^+(\boldsymbol{x})\right\}. \tag{5}$$

It stores the maximum value of the tensile part of the strain energy Ψ_e^+ in each integration point. Finally, the solution of the coupled problem is explained in the last sub-section. For more details about the phase-field approach and its discretization with FEM and FCM, the reader is referred to refs. [1, 6]. The weak forms (Equations 3–4) are discretized, resulting in the residuals

$$\boldsymbol{R}_{\boldsymbol{u}}(\boldsymbol{u},s) = \int_\Omega g(s)\boldsymbol{B}^T\boldsymbol{\sigma}_v(\boldsymbol{u})\,\mathrm{d}\Omega - \left(\int_\Omega \boldsymbol{N}^T\,\boldsymbol{b}\;\mathrm{d}\Omega + \int_{\Gamma_N}\boldsymbol{N}^T\,\bar{\boldsymbol{t}}\;\mathrm{d}\Gamma\right), \tag{6}$$

$$\boldsymbol{R}_s(\boldsymbol{u},s) = \int_\Omega 2\mathcal{H}(\boldsymbol{u})\boldsymbol{N}_s^T(s-1)\;\mathrm{d}\Omega + \int_\Omega G_c\left(\boldsymbol{N}_s^T\frac{s}{\ell} + \ell\,\boldsymbol{B}_s^T\nabla s\right)\mathrm{d}\Omega\,. \tag{7}$$

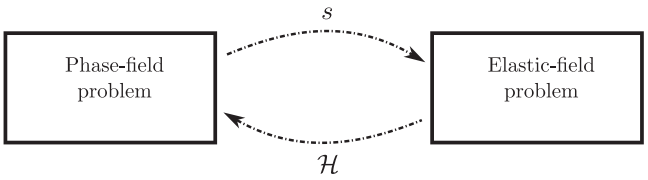

FIGURE 3 Staggered solution scheme for the coupled elastic and phase-field problem.

Here, the displacement field is approximated as $\boldsymbol{u} = \boldsymbol{N}\boldsymbol{U}$ and the strains in Voigt notation as $\boldsymbol{\varepsilon}_v = \boldsymbol{B}\boldsymbol{U}$, where $\boldsymbol{N}$ is the shape function matrix, $\boldsymbol{B}$ the strain-displacement operator and $\boldsymbol{U}$ the unknown solution vector of the displacements. The stresses in Voigt notation then are computed as $\boldsymbol{\sigma}_v = \boldsymbol{C}\boldsymbol{\varepsilon}_v$, where $\boldsymbol{C}$ is the elasticity matrix. Furthermore, the phase-field is approximated as $s = \boldsymbol{N}_s\boldsymbol{S}$ and its gradient as $\nabla s = \boldsymbol{B}_s\boldsymbol{S}$, where $\boldsymbol{N}_s$ is the shape function matrix, $\boldsymbol{B}_s$ the gradient matrix and $\boldsymbol{S}$ the unknown solution vector of the phase-field. The solution of the nonlinear coupled problems (Equations 6)–7) is addressed in the followings.

2.2 | Solution scheme

In order to solve the nonlinear coupled problem, an implicit staggered solution scheme (Figure 3) is utilized, which treats the coupled problem as an alternate minimization problem [12]. It divides the whole problem into two sub-problems: the phase-field problem (Equation 7) and the elastic-field problem (Equation 6). In general, these sub-problems are nonlinear, which are solved by the Newton–Raphson method during each iteration, leading to a huge computational effort. Fortunately, this issue can be overcome, when these sub-systems become linear in terms of the current unknown ($\boldsymbol{u}$ in Equation 6, s in Equation 7). This is the case for linear elasticity of the elastic-field problem as well as a quadratic degradation function for the phase-field problem, which are assumed in this work. The following two mechanisms are responsible for the coupling:

1. material degradation
2. driving force

In contrast to monolithic solution schemes, staggered approaches are more robust and lead to smaller systems of equations [1]. Due to these advantages, staggered schemes are employed in this work.

The implicit staggered solution scheme works as follows: After the initialization, it solves the phase-field problem first (with $\mathcal{H}_{i,j}$ as an input), and uses the output $s_{i,j+1}$ as an input for the elastic-field problem. Once the elastic-field problem is solved, resulting in $\boldsymbol{u}_{i,j+1}$ and the history-fields ($\mathcal{H}_{i,j+1}$), its output is sent again as input to the phase-field problem. These steps are repeated until convergence is achieved, that is the residuals $r_s = \|\boldsymbol{R}_s(\boldsymbol{u}_{i,j+1}, s_{i,j+1})\|_2$ and $r_{\boldsymbol{u}} = \|\boldsymbol{R}_{\boldsymbol{u}}(\boldsymbol{u}_{i,j+1}, s_{i,j+1})\|_2$ both lie below a tolerance ε. This solution scheme is summarized in Algorithm 1.

ALGORITHM 1 Implicit staggered solution scheme

```
Initialize s_0, u_0 → H_{i,0}
for i = 1, ⋯, n_steps do
    Set load
    Initialize s_{i,0}, u_{i,0} → H_{i,0}
    for j = 1, ⋯, j_max do
        Solve phase-field problem (Equation (7))
        Solve elastic field problem (Equation (6)) & update history-field
        Compute residuals (r := max{r_s, r_u})
        if converged (r < ε) then
            break
        end if
    end for
end for
```

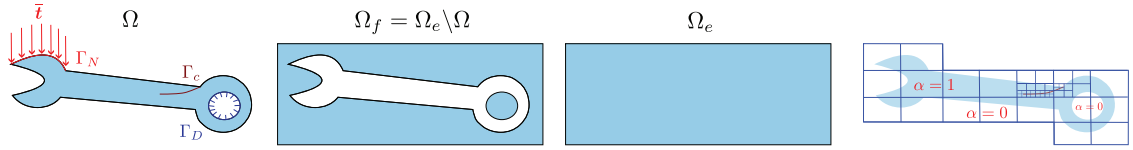

FIGURE 4 Concept of the FCM. Mesh refinement of the crack utilizing the multi-level *hp*-refinement [6, 7]. FCM, finite cell method.

3 | FINITE CELL METHOD

3.1 | Basic formulation

The main idea of the FCM is to embed the physical domain Ω into a simple-shaped domain Ω_e, which can be meshed easily with a Cartesian grid (Figure 4). The fictitious domain $\Omega_f = \Omega_e \setminus \Omega$ is then penalized by the indicator function

$$\alpha(\boldsymbol{x}) = \begin{cases} 1, & \boldsymbol{x} \in \Omega \\ \alpha_0, & \boldsymbol{x} \in \Omega_e \setminus \Omega \,, \end{cases} \tag{8}$$

where $\alpha_0 \ll 1$ is a small parameter ensuring stability in Ω_f [17]. Now, an arbitrary function $f(\boldsymbol{x})$ should be integrated over the physical domain Ω. Due to FCM concept, this is now expressed as

$$\int_{\Omega} f(\boldsymbol{x}) \, \mathrm{d}\Omega = \int_{\Omega_e} \alpha \, f(\boldsymbol{x}) \, \mathrm{d}\Omega \,. \tag{9}$$

This approach is applied to the integrals above in order to simulate the coupled elastic and phase-field problem with FCM. These integrals are discontinuous due to $\alpha(\boldsymbol{x})$, which have to be treated carefully. There exist several methods to solve this problem [8]. One commonly used integration scheme is the adaptive space-tree method (quadtree in 2D / octree in 3D) [5]. They are very robust and accurate, but lead to a huge number of IPs and thus, are very expensive. In order to overcome this issue, moment fitting schemes [9] have been developed, which derive a special quadrature rule (points and weights) for each broken finite cell and thus, strongly reduce the overall number of IPs. These IPs are reused for each iteration and load step of nonlinear and/or coupled problems. However, the simulations then are not robust anymore and even can become unstable, because of possible negative weights and that the IPs lie in the fictitious domain [10]. Therefore, in order to overcome these drawbacks and take the advantages of both schemes (robustness of space-trees, efficiency of moment fitting), the NNMF has been developed recently [10], which will be briefly explained in the followings.

3.2 | Non-negative moment fitting

The NNMF derives a special quadrature rule for each broken finite cell, similar as the standard moment fitting. However, all IPs are located in the physical domain and also are constrained to be positive ($w_i \geq 0$). In general, moment fitting schemes express a function $f(\boldsymbol{x})$ in terms of m basis functions $f_j(\boldsymbol{x})$, $j = 1, \dots, m$. In this work, hierarchical shape functions based on integrated Legendre polynomials are utilized. Given an unknown set of n IPs, each with a weight w_i and position $\boldsymbol{x}_i$, then the following relation holds

$$\sum_{i=1}^{n} w_i \, f_j(\boldsymbol{x}_i) = \int_{\Omega} f_j(\boldsymbol{x}) \, \mathrm{d}\Omega, \quad j = 1, \dots, m. \tag{10}$$

Here, the positions $\boldsymbol{x}_i$ as given, while the moments w_i are unknown. This linear system of equations can be written as

$$\boldsymbol{A}\boldsymbol{w} = \boldsymbol{m} \,, \tag{11}$$

where

$$A_{ji} = f_j(\boldsymbol{x}_i) \tag{12}$$

$$m_j = \int_{\Omega} f_j(\boldsymbol{x}) \, \mathrm{d}\Omega \,. \tag{13}$$

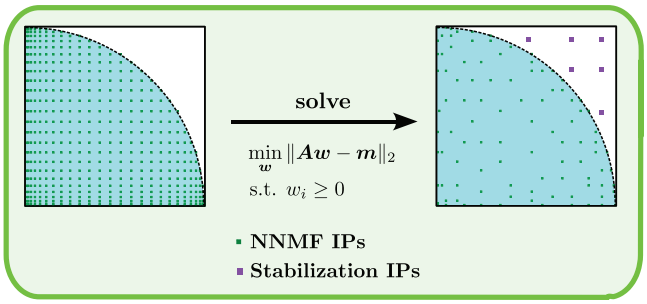

FIGURE 5 Concept of the NNMF scheme. The stabilization points are computed by the α-stabilization [17]. NNMF, non-negative moment fitting.

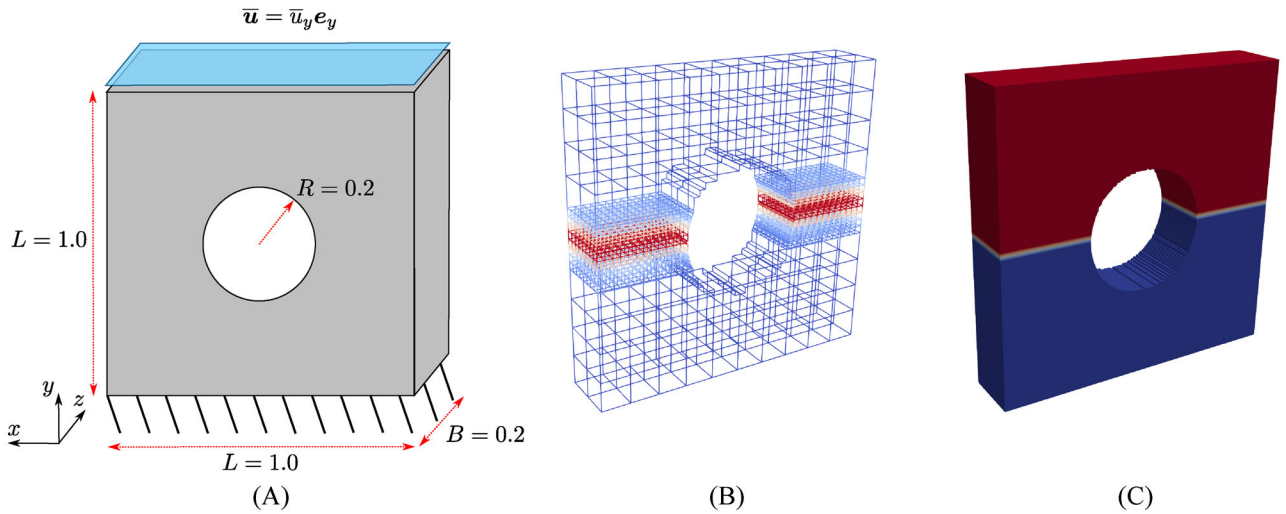

FIGURE 6 Cube with cylindrical hole. (A) Setup of the problem, (B) FCM mesh with phase-field solution s, and (C) displacement solution u_y. All solutions are visualized at the last load step (displacement level: $\bar{u}_y = 0.0112$).

There exist several ways how the moments m_i can be computed. In this work, the adaptive space-tree method is employed in order to compute m_i. The NNMF is illustrated in Figure 5. The major steps of the NNMF are given as follows:

1. Distribution of IPs in physical domain
2. Setup moment fitting system of equations (computation of moments)
3. Solve constrained optimization problem

First, the IPs are distributed in the physical domain with the help of adaptive space-trees [10]. Next, the moment fitting system in Equation (11) is set up, as explained before. Finally, the constrained optimization problem

$$\begin{aligned} &\min_{\boldsymbol{w}} \|\boldsymbol{A}\boldsymbol{w} - \boldsymbol{m}\|_2 \\ &\text{s.t. } w_i \geq 0 \end{aligned} \tag{14}$$

is solved using a non-negative least squares solver [18]. In addition, IPs are distributed in the fictitious domain for stabilization purposes. Further details about the NNMF scheme can be found in ref. [10].

4 | NUMERICAL EXAMPLE: CUBE WITH CYLINDRICAL HOLE (3D)

In this benchmark, a cube with a cylindrical hole under increasing uniaxial tension is investigated (Figure 6A). The proposed FCM phase-field approach as described previously is utilized in order to simulate the problem. A mesh with

TABLE 1 Parameters used in the benchmark.

	Parameter	Value		Parameter	Value
Geometry	L	1.0 mm	FCM setup	$n_x \times n_y \times n_z$	$10 \times 10 \times 2$
	B	0.2 mm		α_0	10^{-6}
	R	0.2 mm		$\mathcal{R}$	3
Material	E	210 000 kN/mm^2		k_{ref}	2
	ν	0.3	Phase-field	ℓ	0.05 mm
	G_c	2.7 N/mm		κ	10^{-6}
Boundary conditions	$\Delta\bar{u}_y$	0.0008 mm	Solver setup	n_{steps}	14
	$\bar{u}_y(i)$	$i \cdot \Delta\bar{u}_y$		$j_{\max}$	100
				ε	10^{-3}

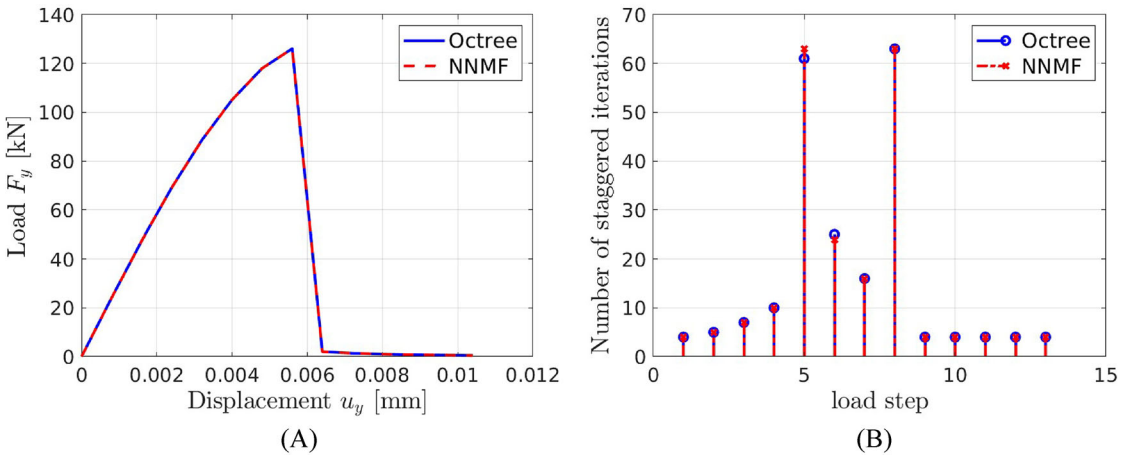

FIGURE 7 Comparison between the octree and NNMF. (A) Load-displacement curve, (B) iteration history.

$10 \times 10 \times 2$ finite cells and multi-level *hp*-refinement with a refinement level of $k_{\text{ref}} = 2$ is utilized (Figure 6B). For the sake of simplicity, all geometry, material and numerical (FCM, phase-field, solver setup) parameters are listed in Table 1. Here, E denotes the Young's modulus of the structure, ν the Poisson ratio, G_c the fracture toughness, ℓ the length-scale parameter and $\Delta\bar{u}_y$ the displacement increment. The prescribed displacement $\bar{u}_y$ rises linearly with the increasing load step i. Furthermore, α_0 and κ are the stabilization parameters, $j_{\max}$ the maximum number of staggered iterations and ε the tolerance.

This example demonstrates that crack initiation can be well predicted by the PFM. When looking at the phase-field solution at the last load step ($i = n_{\text{steps}}$) in Figure 6B, it reaches it maximum at the center plane ($y = L/2$), where failure is observed. This is also reflected in the displacement solution u_y at the last load step ($i = n_{\text{steps}}$) in Figure 6C, which is discontinuous at the same surface ($y = L/2$).

Now, a quantitative study is performed, where the different integration schemes – the octree and the NNMF – should be compared. For both schemes, the tree-depth is given by $\mathcal{R} = 3$. For the octree, $n_G = (2p+1)^3$ IPs per subcell are utilized. The number of moments for the NNMF is given as $m = (4p+1)^3$, which are computed by the octree. The load-displacement curve (Figure 7A) shows an increasing load at larger displacement levels for both methods, until the load suddenly drops. This happens when the structure is fully damaged. Here, the NNMF yields the same results as the octree. Also the number of iterations is very similar between both methods (Figure 7B), where differences are negligible. The number of iterations is in an acceptable region (<30), and reaches high values (~60) only at the critical load steps, that is when the crack starts to propagate. From Figure 7B, it seems as if the computational effort would be similar between both integration schemes. However, the NNMF is around five times faster than the octree (see Table 2). The reason for this is, that the octree needs a very high number of IPs, which can be highly reduced by the NNMF. Here, the NNMF reduced the total number of IPs by a factor of 10. This benchmark reveals that the NNMF is suited very well for FCM fracture computations.

TABLE 2 Computational effort of the octree and NNMF. For each quantity f (in each column), the ratio is given as ratio $= \frac{f_{\text{Octree}}}{f_{\text{NNMF}}}$.

Integration scheme	Number of integration points	Simulation time
Octree	840 024	21 min, 16 s
NNMF	85 144	4 min, 25 s
Ratio	9.9	4.8

5 | CONCLUSIONS

In this work, an immersed computational framework for brittle fracture based on the FCM and PFM has been presented. Furthermore, the NNMF has been employed in order to further accelerate the computations. The proposed approach provides a fast meshing and thus, simplifies the pre-processing. It has been studied on a numerical benchmark. Here, fast and accurate results were obtained by the NNMF, which therefore is a promising approach.

In the future, it is planned to circumvent the mesh refinement at the crack path by enrichment of the Ansatz space. First research has been already conducted in this field, see for example, in ref. [19], and it is gaining more attention in the scientific community.

ACKNOWLEDGMENTS

The authors gratefully acknowledge the support provided by the DFG (Deutsche Forschungsgemeinschaft) under the grant number DU 405/17 with project number 448085183 and grant number DU 405/21 with project number 505137962.

Open access funding enabled and organized by Projekt DEAL.

ORCID

Mahan Gorji https://orcid.org/0000-0002-0722-1573
Seyed Farhad Hosseini https://orcid.org/0000-0002-1219-4629
Roman Sartorti https://orcid.org/0000-0002-3410-8584
Lars Radtke https://orcid.org/0000-0001-7015-8928

REFERENCES

1. De Lorenzis, L., & Gerasimov, T. (2020). *Numerical implementation of phase-field models of brittle fracture* (pp. 75–101). Springer International Publishing.
2. Khadyko, M., Frodal, B. H., & Hopperstad, O. S. (2021). Finite element simulation of ductile fracture in polycrystalline materials using a regularized porous crystal plasticity model. *International Journal of Fracture*, *228*, 15–31.
3. Hug, L., Potten, M., Stockinger, G., Thuro, K., & Kollmannsberger, S. (2022). A three-field phase-field model for mixed-mode fracture in rock based on experimental determination of the mode II fracture toughness. *Engineering and Computing*, *38*, 5563–5581.
4. Borden, M., Verhoosel, C., Scott, M., Hughes, T., & Landis, C. (2012). A phase-field description of dynamic brittle fracture. *Computer Methods in Applied Mechanics and Engineering*, *217-220*, 77–95.
5. Düster, A., Parvizian, J., Yang, Z., & Rank, E. (2008). The finite cell method for three-dimensional problems of solid mechanics. *Computer Methods in Applied Mechanics and Engineering*, *197*, 3768–3782.
6. Nagaraja, S., Elhaddad, M., Ambati, M., Kollmannsberger, S., De Lorenzis, L., & Rank, E. (2019). Phase-field modeling of brittle fracture with multi-level *hp*-FEM and the finite cell method. *Computational Mechanics*, *63*, 1283–1300.
7. Zander, N., Bog, T., Elhaddad, M., Frischmann, F., Kollmannsberger, S., & Rank, E. (2016). The multi-level *hp*-method for three-dimensional problems: Dynamically changing high-order mesh refinement with arbitrary hanging nodes. *Computer Methods in Applied Mechanics and Engineering*, *310*, 252–277.
8. Abedian, A., Parvizian, J., Düster, A., Khademyzadeh, H., & Rank, E. (2013). Performance of different integration schemes in facing discontinuities in the finite cell method. *International Journal of Computational Methods*, *10*, 1350002.
9. Hubrich, S., & Düster, A. (2019). Numerical integration for nonlinear problems of the finite cell method using an adaptive scheme based on moment fitting. *Computers and Mathematics with Applications*, *77*, 1983–1997.
10. Garhuom, W., & Düster, A. (2022). Non-negative moment fitting quadrature for cut finite elements and cells undergoing large deformations. *Computational Mechanics*, *70*, 1059–1081.
11. Francfort, G., & Marigo, J.-J. (1998). Revisiting brittle fracture as an energy minimization problem. *Journal of the Mechanics and Physics of Solids*, *46*, 1319–1342.
12. Bourdin, B., Francfort, G., & Marigo, J.-J. (2008). The variational approach to fracture. *Journal of Elasticity*, *91*, 5–148.

13. Amor, H., Marigo, J.-J., & Maurini, C. (2009). Regularized formulation of the variational brittle fracture with unilateral contact: Numerical experiments. *Journal of the Mechanics and Physics of Solids*, *57*, 1209–1229.
14. Ambati, M., Gerasimov, T., & De Lorenzis, L. (2015). A review on phase-field models of brittle fracture and a new fast hybrid formulation. *Computational Mechanics*, *55*, 383–405.
15. Miehe, C., Welschinger, F., & Hofacker, M. (2010). Thermodynamically consistent phase-field models of fracture: Variational principles and multi-field FE implementations. *International Journal for Numerical Methods in Engineering*, *83*, 1273–1311.
16. Miehe, C., Hofacker, M., & Welschinger, F. (2010). A phase field model for rate-independent crack propagation: Robust algorithmic implementation based on operator splits. *Computer Methods in Applied Mechanics and Engineering*, *199*, 2765–2778.
17. Garhuom, W., Usman, K., & Düster, A. (2022). An eigenvalue stabilization technique to increase the robustness of the finite cell method for finite strain problems. *Computational Mechanics*, *69*, 1225–1240.
18. Lawson, C. L., & Hanson, R. J. (1995). Solving least squares problems. *Society for Industrial and Applied Mathematics*, *15*, https://epubs.siam.org/doi/10.1137/1.9781611971217
19. Loehnert, S., Krüger, C., Klempt, V., & Munk, L. (2023). An enriched phase-field method for the efficient simulation of fracture processes. *Computational Mechanics*, *71*, 1015–1039.

How to cite this article: Gorji, M., Hosseini, S. F., Sartorti, R., Radtke, L., & Düster, A. (2024). Acceleration of immersed computations of brittle phase-field fracture utilizing moment fitting schemes. *Proceedings in Applied Mathematics and Mechanics*, e202400094. https://doi.org/10.1002/pamm.202400094